

Harm J.J. Jonker* and Jérôme Schalkwijk
Delft University of Technology, The Netherlands

ABSTRACT

A mixed layer approach is performed to study the response of convective boundary layers to changing surface conditions. Following the method outlined in van Driel and Jonker (2010) we can analytically derive the internal time-scales of the dynamical boundary layer system (PBL depth, and mixed layer values of temperature and humidity), and hence determine and understand the response to transient conditions in terms of delay and amplitude. The analysis is conducted for different boundary conditions: 1) fixed (i.e. prescribed) surface fluxes for temperature and humidity, 2) interactive fluxes where the fluxes depend on the mixed layer values of temperature and humidity via a transfer velocity, 3) fluxes following from a land-surface energy balance (using the Penman-Monteith equations, see e.g. van Heerwaarden et al. (2009)). It turns out that even in the third, rather complicated, situation, one can analytically derive the three internal time-scales of the dynamical system, which allows one to quantify the relation between the response of the boundary layer and the particular surface properties, solar irradiation and the free-tropospheric conditions. This information provides important insight into the response characteristics of mixed layers to changing conditions, such as governed by the diurnal cycle, but also faster variations due to solar blocking by clouds. The analytical predictions are tested by numerical integration of the mixed layer equations, as well as by a series of Large Eddy Simulations.

1. INTRODUCTION

2. MIXED LAYER MODEL SET-UP

2.1 constant subsidence profile

Following van Driel and Jonker (2010) we study the mixed layer model introduced by Tennekes (1973) in the presence of large scale subsidence. Expanding the original model with non-zero subsidence is both relevant and interesting; it counteracts the growth by entrainment and steady state situations where the PBL-depth gets constant become possible. If one requires that the free troposphere be in a steady state, it is important to also invoke a cooling term R in the temperature equation in order to balance the heating due to subsiding warm air (van Driel and Jonker, 2010). When the free tropospheric potential temperature can be described by a constant lapse rate

*Corresponding author address: Harmen Jonker, Delft University of Technology, Delft, The Netherlands (h.j.jonker@tudelft.nl)

Γ one has $R = w_s \Gamma$, where w_s denotes the value of the subsidence. The mixed layer equations are then given by

$$\frac{d\zeta}{dt} = w_e - w_s \quad (1a)$$

$$\frac{d\theta}{dt} = \frac{\phi - \phi_e}{\zeta} - w_s \Gamma \quad (1b)$$

Using the zero order model of Lilly (1968) the entrainment rate can be expressed in terms of the entrainment flux and inversion strength Δ (flux-jump relation)

$$\phi_e = -w_e \Delta \quad (2)$$

To close the model the entrainment flux is assumed to be a constant fraction of the surface flux (Ball, 1960; Tennekes, 1973)

$$\phi_e = -c\phi \quad (3)$$

where c is the entrainment ratio with a typical value of 0.2-0.3. Combining these equations one has

$$w_e = \frac{c\phi}{\Delta} \quad (4)$$

Contrary to van Driel and Jonker (2010) we will elaborate this model in terms of the mixed layer temperature θ rather than in terms of the jump Δ . For the present model there is no preferable choice, but the models in the sequel find an easier implementation in terms of θ . The relation between the mixed layer temperature and the inversion jump is given by

$$\Delta = \theta^{\text{FT}} + \Gamma\zeta - \theta \quad (5)$$

where θ^{FT} denotes the temperature at the surface when the free tropospheric profile would be extrapolated to the bottom. The governing equations are given by

$$\frac{d\zeta}{dt} = f(\zeta, \theta) = \frac{c\phi}{\theta^{\text{FT}} + \Gamma\zeta - \theta} - w_s \quad (6a)$$

$$\frac{d\theta}{dt} = g(\zeta, \theta) = \frac{(1+c)\phi}{\zeta} - w_s \Gamma \quad (6b)$$

For a constant surface heat flux ϕ , the stationary state are found by setting the time derivatives to zero and solving the resulting coupled equations $f(\tilde{\theta}, \tilde{\zeta}) = g(\tilde{\theta}, \tilde{\zeta}) = 0$, which yields a unique solution

$$\begin{aligned} \tilde{\zeta} &= \frac{(1+c)\phi}{w_s \Gamma} \\ \tilde{\theta} &= \theta^{\text{FT}} + \frac{\phi}{w_s} \end{aligned} \quad (7)$$

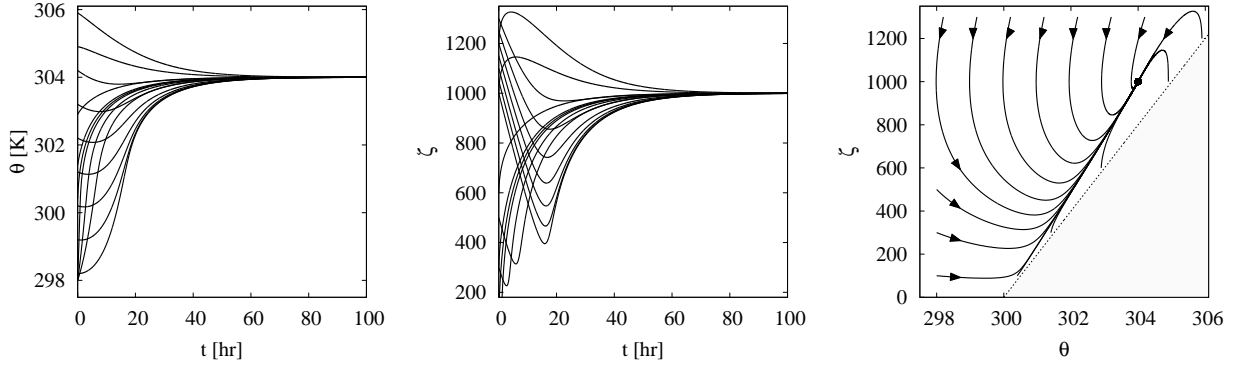


FIG. 1: Evolution of $\theta(t)$ (left) and $\zeta(t)$ (middle) as a function of time for different initial conditions. Right: trajectories in $(\theta(t), \zeta(t))$ phase-space. For the parameter settings, see Table 1, case I. The fixed point is indicated by the circle. The gray region below the dashed line is not admissible, as it corresponds to negative inversion jumps Δ . The thick line illustrate the slow direction in the system: trajectories first converge onto this curve followed by a slow progression towards the steady state.

The local stability of the fixed point follows from the Jacobian \mathbf{J} evaluated at the fixed point, where in general \mathbf{J} is given by

$$\mathbf{J}(\zeta, \theta) = \begin{bmatrix} \frac{\partial f}{\partial \zeta} & \frac{\partial f}{\partial \theta} \\ \frac{dg}{d\zeta} & \frac{dg}{d\theta} \end{bmatrix} \quad (8)$$

The Jacobian in the fixed point (7), $\tilde{\mathbf{J}} = \mathbf{J}(\tilde{\zeta}, \tilde{\theta})$ is found to be

$$\tilde{\mathbf{J}} = -\frac{1}{\tau_s} \begin{bmatrix} 1+c & -\frac{1+c}{c\Gamma} \\ \Gamma & 0 \end{bmatrix} \quad (9)$$

where we have defined the overall time-scale

$$\tau_s = \frac{\tilde{\zeta}}{w_s} \quad (10)$$

Eigenvalues of $\tilde{\mathbf{J}}$ provide information on the stability of the fixed point. When the real part of the eigenvalues is negative, the fixed point is (at least locally) stable to perturbations and forms an attractor. When the real part is positive the fixed point is unstable to perturbations and acts as a repeller. Solving the eigenvalue problem yields

$$\lambda_{\pm} = -\frac{1}{\tau_s} \left[\frac{1+c \pm \sqrt{(1+c)(1-3c)}}{2c} \right] \quad (11)$$

Eq. (11) thus reveals that the fixed point (7) is always stable since $c > 0$. In addition (11) give the time scale(s) associated with exponential decay $\sim \exp(-t/\tau_{\pm})$ to the fixed point; so $\tau_{\pm} = -1/\text{Re}(\lambda_{\pm})$. For $0 < c < 1/3$ there are two real eigenvalues and therefore two time scales in the system. For example, if $c = 0.2$, the two time scales are

$$\tau_{1,2} = -\frac{1}{\lambda_{\pm}} = \frac{\tau_s}{3 \pm \sqrt{3}} \approx 0.22\tau_s, 0.78\tau_s \quad (12)$$

If $c > 1/3$, the eigenvalues are complex valued, implying the system will exhibit a damped oscillation $\sim \exp(-t/\tau_{\pm} \pm i\omega t)$, where

$$\tau = \frac{2c}{1+c}\tau_s \quad \omega = \tau_s^{-1} \frac{\sqrt{(1+c)(3c-1)}}{2c} \quad (13)$$

It is important to note that the time scales and frequencies in (12) and (13) scale with τ_s given by (10). Substituting typical values like $\tilde{\zeta} \simeq 10^3 \text{m}$ and $w_s = 10^{-2} \text{m/s}$, one obtains $\tau_s = 10^5 \text{s} \approx 24 \text{hr}$. It demonstrates how slow the dynamics of the PBL depth is (van Driel and Jonker, 2010); it is definitely not governed by the time scale of turbulence $t_* = \zeta/w_*$ which is typically two orders of magnitude smaller. Rather the system is governed by ζ/w_e , the PBL depth and the *entrainment* velocity; in steady state this time scale amounts to τ_s given in (10).

Fig. 1 shows the evolution of the system for various initial conditions. The used system parameters are listed in Table 1. In the phase-plot (right) one can nicely observe the convergence to the stable fixed point. Fig. 2 show LES results for the same case. Apparently the agreement is quite good, certainly in a qualitative sense.

2.2 alternative subsidence profile: divergence

Since the subsidence w_s plays a prominent role in the time scale(s) of the system, viz. Eqs. (12,13), it is interesting to study an alternative subsidence profile; a relevant choice is to express the subsidence in terms of a divergence D : $w_s(z) = Dz$. Because of the requirement that the free troposphere is in steady state, the cooling term in the temperature equation must be height-dependent as well $R(z) = -D\Gamma z$. Consistent application in the mixed layer entails averaging over the ζ , hence a temperature sink of $-D\Gamma\zeta/2$. The system equations be-

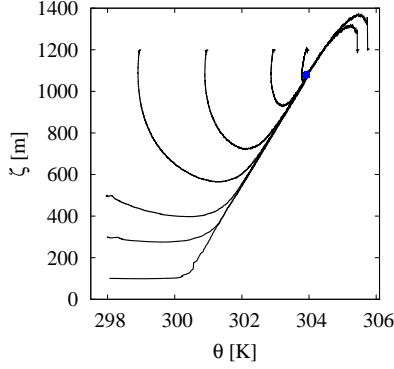


FIG. 2: LES results corresponding to case I (see Table 1). Compare with Fig. 1.

come

$$\frac{d\zeta}{dt} = w_e - D\zeta \quad (14a)$$

$$\frac{d\theta}{dt} = \frac{(1+c)\phi}{\zeta} - \frac{1}{2}D\Gamma\zeta \quad (14b)$$

in conjunction with (4) and (5). D, ϕ, Γ are the system parameters. The fixed point is

$$\begin{aligned} \tilde{\zeta} &= \sqrt{\frac{2(1+c)\phi}{D\Gamma}} \\ \tilde{\theta} &= \theta^{\text{FT}} + \frac{(2+c)\phi}{D\tilde{\zeta}} \end{aligned} \quad (15)$$

The Jacobian evaluated at the fixed point is

$$\tilde{\mathbf{J}} = -D \begin{bmatrix} \frac{2+3c}{c} & -\frac{2(1+c)}{c\Gamma} \\ \Gamma & 0 \end{bmatrix} \quad (16)$$

with eigenvalues

$$\lambda_1 = -D \quad \lambda_2 = -D \frac{2(1+c)}{c} \quad (17)$$

Both eigenvalues are both real and negative, so the fixed point (15) is unconditionally stable. Also, because both eigenvalues are real valued regardless of the value of c , there are no oscillatory solutions. The overall time scale is $\tau_s = \tilde{\zeta}/w_s = 1/D$. There is fast mode (associated with λ_2) which, for $c = 1/4$, is about *ten* times faster than the slow mode which has time scale $\tau = D^{-1}$. With a typical value of $D \simeq 10^{-5}\text{s}^{-1}$, this time scale is in the order of 24hr. Fig. 3 shows dynamics for parameters values $D = 3 \cdot 10^{-5}\text{s}^{-1}$, $\phi = 0.06\text{Kms}^{-1}$, $\Gamma = 5\text{Km}^{-1}$, $\theta^{\text{FT}} = 300\text{K}$. The time scales are $\tau_1 = 1/\lambda_1 \simeq 10\text{hr}$, $\tau_2 = 1/\lambda_2 \simeq 1\text{hr}$, respectively. Indeed, the evolution of $\zeta(t)$ and $\theta(t)$ is somewhat faster than in Fig. 1, consistent with the calculated values of τ . The trajectories in phase space reveal the relatively fast convergence of the trajectories onto the thick line, followed by much slower convergence to the fixed point (circle).

Apart from minor quantitative differences between the graphs in Fig. 3 and the constant subsidence version in Fig. 1, the overall dynamical character appears to be very similar, leading one to conclude that the different choices for the subsidence profile entail no drastic effects qualitatively. With this in mind, in the sequel we will therefore revert to the constant subsidence setting.

3. COUPLED SURFACE FLUX

In this section we explore the situation where the surface heat flux is not prescribed but coupled to the mixed layer temperature

$$\phi = -w_t(\theta - \theta_s) \quad (18)$$

where θ_s represents the (prescribed) surface temperature and w_t a transfer coefficient. Depending on one's taste one can think of w_t as a resistance $w_t = 1/r_a$ (van Heerwaarden et al., 2009), or as a drag-law $w_t = C_d U$. The system is now given by:

$$\frac{d\zeta}{dt} = w_e - w_s \quad (19a)$$

$$\frac{d\theta}{dt} = w_t \frac{(1+c)(\theta_s - \theta)}{\zeta} - w_s \Gamma \quad (19b)$$

which is to be solved together with the entrainment closure (4), the jump relation (5), and (18); the independent external parameters are $w_s, \Gamma, w_t, \theta_s$. Assuming a stationary surface temperature θ_s , the unique fixed point of the system is

$$\begin{aligned} \tilde{\zeta} &= \frac{w_t(1+c)(\theta_s - \theta^{\text{FT}})}{(w_t + w_s)\Gamma} \\ \tilde{\theta} &= \frac{w_s \theta^{\text{FT}} + w_t \theta_s}{w_t + w_s} \end{aligned} \quad (20)$$

The local stability of the fixed point follows from the Jacobian evaluated at the fixed point, which is found to be

$$\tilde{\mathbf{J}} = -\frac{1}{\tau_s} \begin{bmatrix} \frac{1+c}{c} & \frac{1+c}{\Gamma} \left[\frac{w_t}{w_s} - \frac{1}{c} \right] \\ \Gamma & (1+c) \frac{w_t}{w_s} \end{bmatrix} \quad (21)$$

and $\tau_s = \tilde{\zeta}/w_s$. It should be noted that τ_s has a w_t -dependence as well through $\tilde{\zeta}$. The eigenvalues of the Jacobian, which reveal the stability of the fixed point, are

$$\begin{aligned} \lambda_{\pm} &= -\frac{1}{\tau_s} \frac{1+c}{2} \left[\left(\frac{w_t}{w_s} + \frac{1}{c} \right) \pm \right. \\ &\quad \left. \sqrt{\left(\frac{w_t}{w_s} - \frac{1}{c} \right) \left(\frac{w_t}{w_s} - \frac{1-3c}{(1+c)c} \right)} \right] \end{aligned} \quad (22)$$

Also in this case the real parts of the eigenvalues are always negative which implies that the fixed point is unconditionally stable.

There are two noteworthy differences with the fixed flux system: Firstly, the time scales are shortened in the coupled flux case; the relative extent with which the time

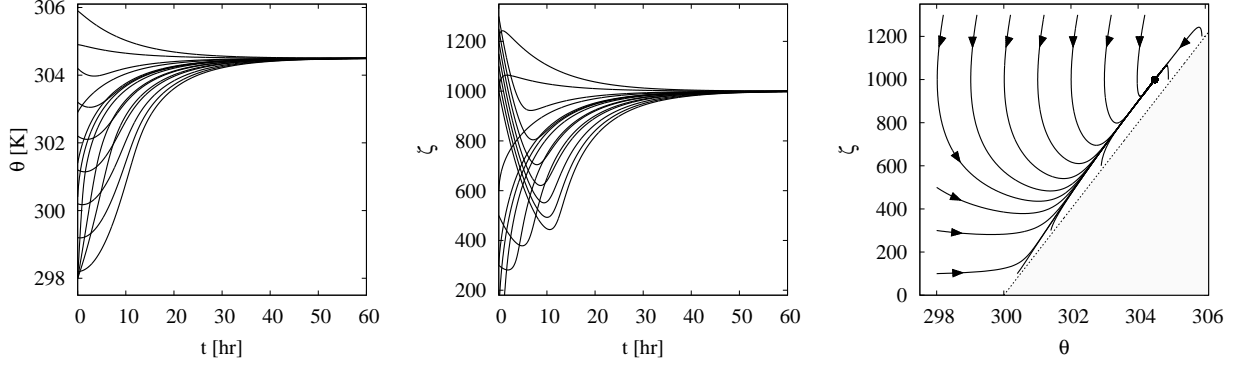


FIG. 3: Evolution of $\theta(t)$ (left) and $\zeta(t)$ (middle) as a function of time for different initial conditions. Right: trajectories in $(\theta(t), \zeta(t))$ phase-space. For the parameter settings, see Table 1, case II. See also the caption of Fig. 1.

case	I (Fig.1)	II (Fig.3)	III (Fig.5)
subsidence	$\bar{w} = -w_s$ $w_s = 0.015\text{ms}^{-1}$	$\bar{w} = -Dz$ $D = 3 \cdot 10^{-5}\text{s}^{-1}$	$\bar{w} = -w_s$ $w_s = 0.015\text{ms}^{-1}$
boundary-condition	$\phi = \phi_0$ $\phi_0 = 0.06\text{Kms}^{-1}$	$\phi = \phi_0$ $\phi_0 = 0.06\text{Kms}^{-1}$	$\phi = -w_t(\theta - \theta_s)$ $w_t = 0.03\text{ms}^{-1}$ $\theta_s = 306\text{K}$
steady st. $\tilde{\zeta}$	1000m	1000m	1000m
steady st. $\tilde{\theta}$	304K	304.5K	304K
timescales	$\tau_1 \simeq 5\text{hr}$ $\tau_2 \simeq 13\text{hr}$	$\tau_1 \simeq 1\text{hr}$ $\tau_2 \simeq 10\text{hr}$	$\tau \simeq 5\text{hr}$ $\omega^{-1} \simeq 19\text{hr}$

Table 1: Parameter settings. In all cases $c = 1/4$, $\theta^{\text{FT}} = 300\text{K}$, $\Gamma = 5 \cdot 10^{-3}\text{Km}^{-1}$

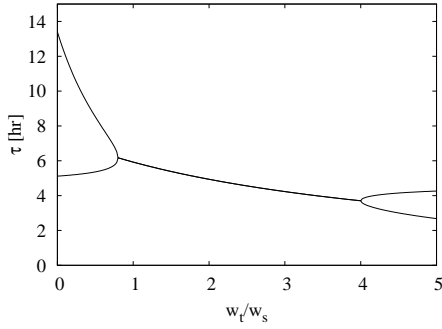


FIG. 4: Dependence of time scales on the (relative) transfer coefficient w_t/w_s . Solid lines: Time scales $\tau_{1,2}$ of the coupled flux system based on the real part of the eigenvalues (22). Settings $c = 1/4$, $\theta^{\text{FT}} = 300\text{K}$, $\Gamma = 5 \cdot 10^{-3} \text{Km}^{-1}$, $w_s = 0.015 \text{ms}^{-1}$. For each w_t the surface temperature θ_s was chosen such that the steady state mixed layer depth $\zeta = 1000\text{m}$.

scale is shortened depends on the magnitude of w_t/w_s and one may note that taking the limit $w_t \rightarrow 0$ in (22) yields the eigenvalues of the prescribed flux case (11) (Taking the limit properly requires one to keep ϕ fixed in order to degenerate to the prescribed flux system). Secondly (damped) oscillatory behaviour can occur in the coupled system for a wider range of c values. Indeed, (22) reveals that the eigenvalues become complex valued when

$$\frac{1-3c}{(1+c)c} < \frac{w_t}{w_s} < \frac{1}{c}$$

For $c = 1/4$, for example, this means oscillatory behaviour when $w_t/w_s \in (0.8, 4)$. Fig. 4 shows the time scales $\tau_{1,2} = 1/\Re\{\lambda_{\pm}\}$, given by (22), as a function of w_t/w_s for $c = 1/4$. For each value of w_t the surface temperature was adapted so as to give $\zeta = 1\text{km}$, which enables a fair comparison with the other cases considered. One notices the collapse of the real parts of the eigenvalues between 0.8 and 4 due to the non-zero imaginary part $i\omega$.

To show the behaviour of the system we present in Fig. 5 the dynamics for $w_t/w_s = 2$, $w_s = 0.015 \text{ms}^{-1}$, $w_t/w_s = 2$, $\theta_s = 306\text{K}$, $\Gamma = 5 \text{Km}^{-1}$, $\theta^{\text{FT}} = 300\text{K}$, which gives $\zeta = 1000\text{m}$, $\hat{\theta} = 304\text{K}$, i.e. similar values as in Fig. 1. Apart from the oscillation frequency there is only one time scale that governs the convergence to the fixed point $\tau \simeq 5\text{hr}$, which is significantly shorter than in the prescribed flux case of section 2.1; compare in particular the left or middle panels of Fig. 5 and Fig. 1, respectively.

One may wonder whether a further increase of the transfer velocity w_t will continue to reduce the time scales of the system, but Fig.4 shows that there is an adverse effect when w_t/w_s exceeds $1/c$ (4 in this example): beyond this value one of the time scales increases with w_t/w_s .

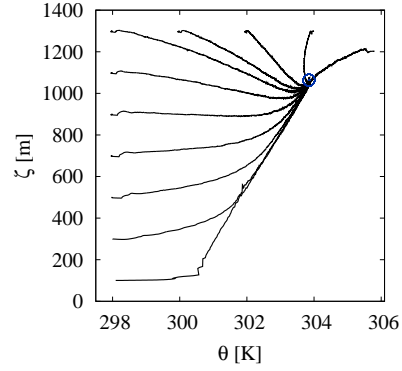


FIG. 6: LES results corresponding to case III (see Table 1). Compare with Fig. 5.

4. GENERALISATION TO LARGER SYSTEMS: INCLUSION OF PASSIVE AND ACTIVE VARIABLES

In this section we increase the order of the system by including an extra quantity χ , which can be passive (like a trace gas such as CO_2) or active (like moisture). The generic system is given by

$$\frac{d\zeta}{dt} = w_e - w_s \quad (23a)$$

$$\frac{d\theta_v}{dt} = \frac{(1+c)\phi_v}{\zeta} - w_s\Gamma_v \quad (23b)$$

$$\frac{d\chi}{dt} = \frac{\phi_\chi + w_e\Delta_\chi}{\zeta} - w_s\Gamma_\chi \quad (23c)$$

Here ϕ_χ represents the surface flux of χ . The inversion jump of χ is denoted by $\Delta_\chi = \chi^{\text{FT}} + \Gamma_\chi\zeta - \chi$, with Γ_χ the tropospheric lapse rate. The term $-w_s\Gamma_\chi$ balances the action of subsidence in the free troposphere, which is assumed to be also in steady state with respect to χ . Note also that we have now used virtual potential temperature θ_v instead of θ as in previous sections. This distinction will be important when we include moisture in the system, which also exerts an effect on buoyancy and therefore also on the entrainment rate

$$w_e = \frac{c\phi_v}{\Delta_v} \quad (24)$$

with ϕ_v the surface buoyancy flux and Δ_v the inversion jump of θ_v ; (24) thus generalizes (4) when moisture comes into play (sections 4.3 and 5).

Below we will study three cases: first, we deal with the case of a passive scalar (tracer gas) which has no coupling to the ζ dynamics; next, we investigate what happens when an equation is included for the mean wind while accounting for the effect of wind on the surface fluxes; finally, we include the effect of moisture on buoyancy. This analysis paves the way to the more complicated case studied in section 5 of land-atmosphere coupling via a surface energy balance.

Before we focus on the specific examples, we first

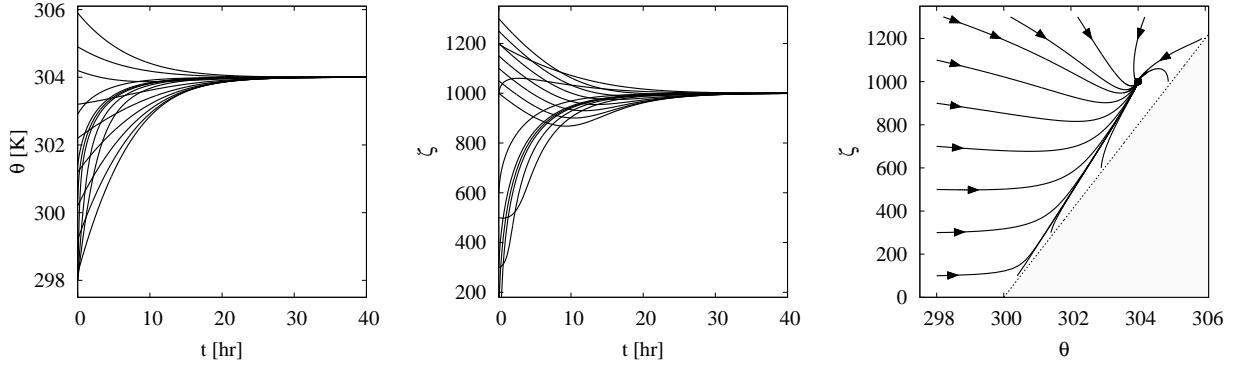


FIG. 5: Evolution of $\theta(t)$ (left) and $\zeta(t)$ (middle) as a function of time for different initial conditions. Right: trajectories in $(\theta(t), \zeta(t))$ phase-space. For the parameter settings, see Table 1, case III. See also the caption of Fig. 1.

note that in all cases the fixed point $\tilde{\chi}$ satisfies the relation

$$\tilde{\phi}_\chi = -w_s(\chi^{\text{FT}} - \tilde{\chi}) \quad (25)$$

which follows from setting $d\chi/dt = 0$ in (23c) together with $\tilde{w}_e = w_s$. The final result for $\tilde{\chi}$ depends on the particular expression for the surface flux. For instance, when the surface flux ϕ_χ is prescribed (fixed), $\tilde{\chi} = \chi^{\text{FT}} + \phi_\chi/w_s$. For the interactive case of $\phi_\chi = -w_t(\chi - \chi_s)$, the fixed point has a form analogous to (20): $\tilde{\chi} = (w_s\chi^{\text{FT}} + w_t\chi_s)/(w_t + w_s)$.

In appendix A we derive the generic Jacobian matrix for the third-order system ζ, θ_v, χ , which is appreciably more involved than the two-dimensional systems considered so far. For the analyses below it will be convenient to define the following derivatives of the fluxes in *steady state*

$$\begin{aligned} P_{vv} &= -\frac{1}{w_s} \frac{\partial \phi_v}{\partial \theta_v} & P_{v\chi} &= -\frac{1}{w_s} \frac{\partial \phi_v}{\partial \chi} \\ P_{\chi v} &= -\frac{1}{w_s} \frac{\partial \phi_\chi}{\partial \theta_v} & P_{\chi\chi} &= -\frac{1}{w_s} \frac{\partial \phi_\chi}{\partial \chi} \end{aligned} \quad (26)$$

4.1 Passive scalar

When χ is a passive scalar, such as for example CO_2 ((Vilà-Guerau de Arellano et al., 2004)), then buoyancy is not influenced by χ . In such a case the dynamical system (ζ, θ_v) is not influenced by χ , yet χ is influenced by ζ and θ_v . So we have $P_{\chi v} = 0$, and $P_{v\chi} = 0$, by (26), which is substituted in (55). The corresponding eigenvalues are (see Appendix A).

$$\lambda_{1,2} = -\frac{1}{\tau_s} \frac{1+c}{2} \left[\left(P_{vv} + \frac{1}{c} \right) \pm \sqrt{\left(P_{vv} - \frac{1}{c} \right) \left(P_{vv} - \frac{1-3c}{(1+c)c} \right)} \right] \quad (27)$$

$$\lambda_\chi = -\frac{1}{\tau_s} [P_{\chi\chi} + 1] \quad (28)$$

Equation (27) generalizes the earlier results of sections 22.1 and 3: Indeed, when the surface buoyancy flux ϕ_v is prescribed, then $P_{vv} = 0$ and (27) simplifies to (11); on the other hand, for an interactive surface flux $\phi_v = -w_t(\theta_v - \theta_{vs})$, one has $P_{vv} = w_t/w_s$, and (27) equals (22). Expression (27) is also valid for other choices of ϕ_v , where the relevant quantity is P_{vv} (together with determination of the fixed points of course).

As regards to the time scale belonging to the dynamics of passive scalar χ , $\tau_\chi = -1/\text{Re}(\lambda_\chi)$, equation (28) shows that besides $\tau_s = \tilde{\zeta}/w_s$ it is only related to $P_{\chi\chi}$. A prescribed surface flux ($P_{\chi\chi} = 0$) gives $\tau_\chi = \tau_s$. For an interactive flux of the form $\phi_\chi = -w_t(\chi - \chi_s)$, it is $\tau_\chi = \tilde{\zeta}/(w_s + w_t)$. In the former case, the value of the flux ϕ_χ does not influence the time scale. In the latter case (interactive flux), an increased transfer rate does reduce τ_χ , even though it has no impact on the overall PBL-dynamics (ζ, θ_v) .

4.2 Wind-flux interactions

In the same vein as done for trace gases one can study the dynamics of mean wind u in the mixed layer simply by setting $\chi = u$. (23c) then yields a prognostics equation for the wind

$$\frac{du}{dt} = \frac{\phi_u + w_e \Delta_u}{\zeta} \quad (29)$$

where we have set $\Gamma_u = 0$; the velocity jump at the inversion is then $\Delta_u = u^{\text{FT}} - u$ with u^{FT} the tropospheric (geostrophic) wind. When u is assumed not to influence the (ζ, θ_v) dynamics, the results for $\chi = u$ are identical to those of passive scalars discussed section 4.1.

An interesting coupling, however, could be one where u is thought to influence surface fluxes via a drag coefficient c_d , e.g.

$$\phi_v = -c_d |u| (\theta_v - \theta_{vs}) \quad (30)$$

and hence also

$$\phi_u = -c_d |u| u \quad (31)$$

Here $-c_d|u|u$ represents the surface momentum flux (drag). Equations (30) and (31) are then to be solved in conjunction with (23) with $\chi = u$.

The fixed point for u follows directly from (29), taking for the steady state entrainment rate $\tilde{w}_e = w_s$ (which follows from (23a)); careful treatment of the signs of u and u^{FT} shows that only one solution is admissible

$$\tilde{u} = \frac{1}{2} \frac{w_s}{c_d} \left[-1 + \sqrt{1 + \frac{c_d}{w_s} |u^{FT}|} \right] \text{sign}(u^{FT}) \quad (32)$$

This sets the equilibrium transfer velocity $w_t = c_d |\tilde{u}|$

$$w_t = \frac{1}{2} \left[\sqrt{w_s(w_s + c_d |u^{FT}|)} - w_s \right]$$

(compare (18)) and as a result, the fixed points $\tilde{\zeta}$, $\tilde{\theta}_v$ are readily derived from expression (20).

Getting the stability and time scales of the system is somewhat more involved, see appendix A, since the characteristic polynomial determining the eigenvalues is now third order. But it is interesting to note that the equation for the rescaled eigenvalues $\mu = \lambda \tau_s$ does solely depend on c and $p = c_d \tilde{u} / w_s$, i.e. the normalized transfer rate. For example for $c = 1/4$ it reads

$$4\mu^3 - 3(3p+8)\mu^2 + 5(2p^2+9p+8)\mu - 20(2p^2+3p+1) = 0 \quad (33)$$

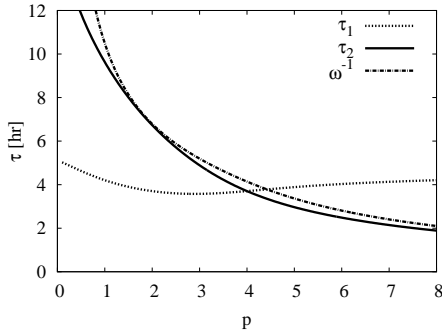


FIG. 7: Dependence of time scales on the normalized transfer coefficient $p = c_d \tilde{u} / w_s$. Solid lines: Time scales $\tau_{1,2}$ based on the real part of the eigenvalues

Fig. 7 shows the timescales $\tau = -\tau_s / \text{Re}(\mu)$ as well as the oscillation period $T = 2\pi\tau_s / \text{Im}(\mu)$. One notices that for the range depicted one of the eigenvalues is real, and two are complex. Calculation of the roots of (33) for general p can be conveniently performed with a symbolic math program such as maple or mathematica, but the resulting expression is too long to present here. An example of the trajectories in the (u, ζ) phase space is given in Fig. 8.

4.3 combining moisture and temperature: a case over sea

When moisture and temperature both play an active role, it seems natural to study the separate prognostic equa-

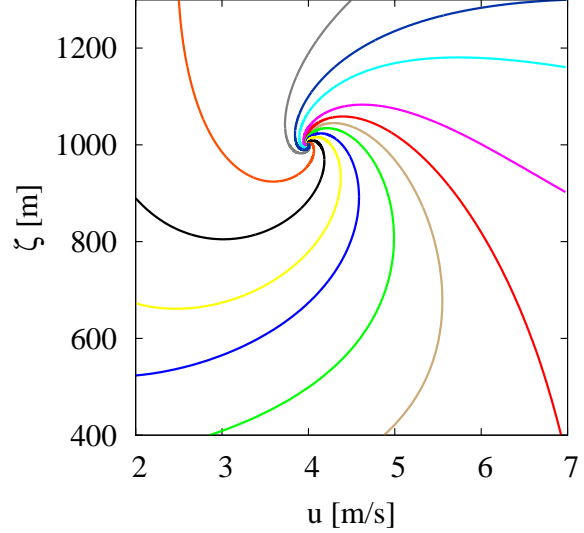


FIG. 8: Trajectories in $u(t), \zeta(t)$ phase space.

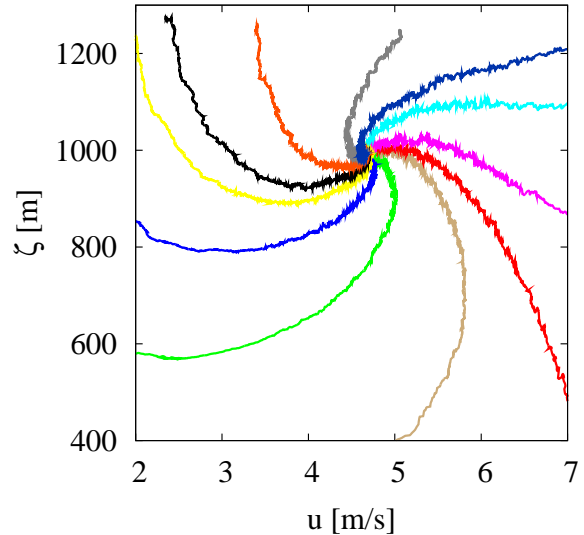


FIG. 9: LES

tions for potential temperature θ and specific humidity q , together with (23a) and (24)

$$\frac{d\theta}{dt} = \frac{\phi_\theta + w_e \Delta_\theta}{\zeta} - w_s \Gamma_\theta \quad (34a)$$

$$\frac{dq}{dt} = \frac{\phi_q + w_e \Delta_q}{\zeta} - w_s \Gamma_q \quad (34b)$$

But a complication resides in the fact that both quantities influence buoyancy, and therefore both exert an effect on the entrainment rate w_e . It turns out to be much more convenient to work with the virtual potential temperature $\theta_v = \theta(1 + \epsilon_I q)$, where $\epsilon_I = R_v/R_d$ (table 2). Throughout the rest of this paper we will employ the approximation

$$\theta_v = \theta + \beta q \quad (35)$$

with $\beta = \theta \epsilon_I \simeq 180$ fixed. Then also

$$\phi_v = \phi_\theta + \beta \phi_q, \quad \Gamma_v = \Gamma_\theta + \beta \Gamma_q \quad (36)$$

The entrainment rate (24) can then be determined by $\Delta_v = \Delta_\theta + \beta \Delta_q$. So rather than system (34), we prefer to study the generic system (23) based on θ_v . For the variable χ one may choose either θ , q , or a linear combination of θ and q .

Suppose one is interested in a case over sea, where the surface temperature and humidity fluxes are parameterized to depend on the sea surface temperature θ_s via

$$\phi_\theta = -w_t[\theta - \theta_s], \quad \phi_q = -w_t[q - q_s] \quad (37)$$

with $q_s = q_{\text{sat}}(\theta_s)$, the saturation humidity corresponding to θ_s . Upon defining the surface buoyancy $\theta_{vs} = \theta_s + \beta q_s$ one can express the surface buoyancy flux as

$$\phi_v = -w_t[\theta_v - \theta_{vs}] \quad (38)$$

The essential point now is that χ does not couple back in any way to equations (23a) and (23b). Fixed points and stability therefore follow directly from the results obtained in section 44.1. The eigenvalues are given by Eqs. (27) and (28), with $P_{vv} = P_{\chi\chi} = w_t/w_s$. In fact the ζ, θ_v system is identical to the one studied in section 3. The extra time scale for χ , which represents q or θ , or a linear combination of both, follows from (28) and is given by $\tau_\chi = \tilde{\zeta}/(w_s + w_t)$.

Whilst this result is straightforward, it should be noted that it only works because the fluxes in (37) are coupled to the surface *by the same transfer velocity* w_t . Should the transfer rates be different, then (38) is no longer valid and an extra term will pop up containing χ . As such χ is no longer decoupled from the ζ, θ_v dynamics, which complicates matters considerably. This will be the topic of the next section.

5. LAND-ATMOSPHERE INTERACTION SOLVING A SURFACE ENERGY BALANCE

In this section we analyse the case studied recently by (van Heerwaarden et al., 2009) of a mixed layer where

the temperature and humidity fluxes follow from a surface energy balance

$$R = G + H + L_E \quad (39)$$

where R represents the incoming solar radiation (in Wm^{-2}), G the ground flux, and $H = \rho c_p \phi_\theta$, $L_E = \rho L_v \phi_q$ the sensible and latent heat respectively. Both fluxes are coupled to the mixed state via

$$\phi_\theta = -w_\theta[\theta - \theta_s], \quad \phi_q = -w_q[q - q_s] \quad (40)$$

where it is important to emphasize that w_θ and w_q can be different; if they were to have the same value, the analysis would simplify considerably as was outlined in section 34.3. But such a simplification is not justified. Note that frequently one uses resistances rather than transfer rates. For example, (van Heerwaarden et al., 2009) used $w_\theta = 1/r_a$, $w_q = 1/(r_a + r_s)$ where r_a is the aerodynamic resistance and r_s the stomatal resistance. At any rate, $w_\theta \neq w_q$.

Just as for the case over sea, one assumes for the saturation value for the surface humidity, $q_s = q_{\text{sat}}(\theta_s)$, which renders θ_s as the only unknown. Following the ideas of Penmann-Monteith (see e.g. van Heerwaarden et al. (2009)), one can further eliminate θ_s and express the temperature and humidity fluxes as a function of $Q = R - G$ (the net energy input), and the mixed layer values of θ and q :

$$\phi_\theta(\theta, q) = \left[\frac{Q}{\rho c_p} - \frac{L_v}{c_p} w_q [q_{\text{sat}}(\theta) - q] \right] \frac{1}{\gamma} \quad (41)$$

$$\phi_q(\theta, q) = \left[w_q [q_{\text{sat}}(\theta) - q] + \frac{Q}{\rho c_p} \frac{w_q}{w_\theta} s(\theta) \right] \frac{1}{\gamma} \quad (42)$$

$$\gamma = 1 + \frac{L_v}{c_p} \frac{w_q}{w_\theta} s(\theta), \quad s(\theta) = \frac{dq_{\text{sat}}}{d\theta} \quad (43)$$

As a check one may note that the fluxes satisfy energy conservation $\rho c_p \phi_\theta + \rho L_v \phi_q = Q$. For the saturation humidity we adopt same expression as used in DALES (Heus et al., 2010)

$$q_{\text{sat}}(\theta) = \frac{R_d}{R_v} \left[\frac{p}{e_s(\theta)} + \frac{R_d}{R_v} - 1 \right]^{-1} \quad (44)$$

$$e_s(\theta) = e_{s0} \exp \left[a \frac{\theta - \theta_{\text{trip}}}{\theta - \theta_b} \right] \quad (45)$$

with constants given in Table 2.

The system is now complete when we add the governing equations for the mixed layer values, e.g. equations (34). Setting the time derivative to zero, one finds that the fixed points can be determined by (numerically) solving the rather complicated non-linear equation set

$$\phi_\theta(\tilde{\theta}, \tilde{q}) = -w_s(\tilde{\theta}^{\text{FT}} - \tilde{\theta}) \quad (46)$$

$$\phi_q(\tilde{\theta}, \tilde{q}) = -w_s(q^{\text{FT}} - \tilde{q}) \quad (47)$$

where the fluxes $\phi_\theta(\tilde{\theta}, \tilde{q})$, $\phi_q(\tilde{\theta}, \tilde{q})$ are given by equations (41-45).

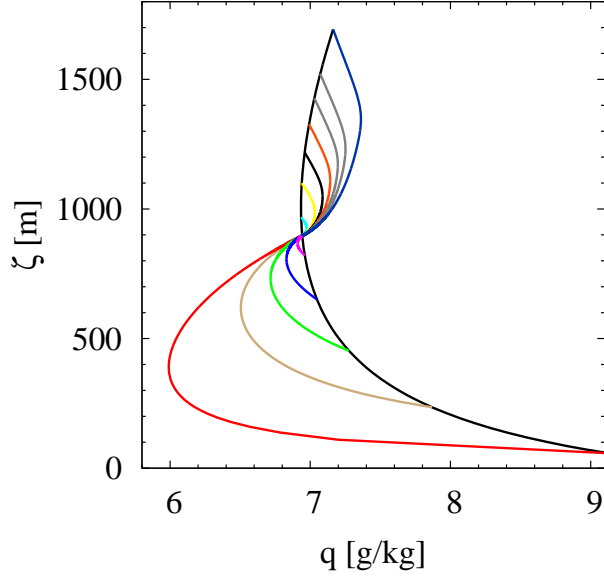


FIG. 10: Phase space plot of q_t, ζ for $Q = 200 \text{ W m}^{-2}$ starting from different initial values of Q .

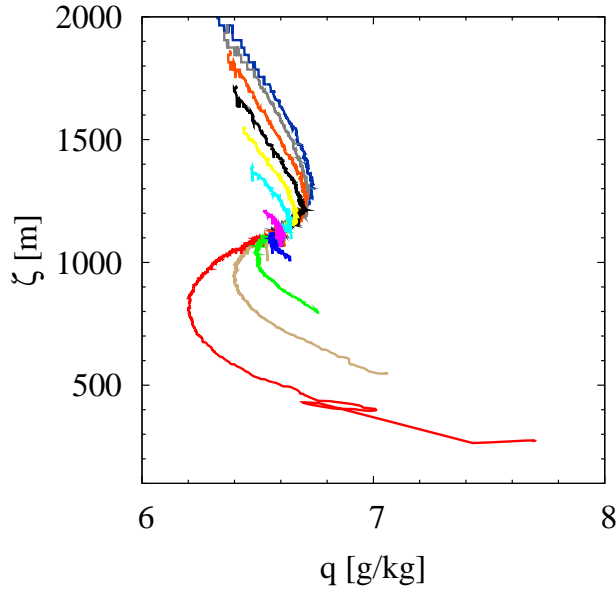


FIG. 11: LES results. Compare Fig. 10.

quantity	value	unit
p	10^5	Pa
e_{s0}	610.78	hPa
θ_{trip}	273.16	K
a	17.27	-
θ_b	35.86	K
R_d	287.04	
R_v	461.5	
ρ	1.2	kg m^{-3}
c_p	1004	$\text{JK}^{-1}(\text{kg})^{-1}$
L_v	$2.5 \cdot 10^6$	JK^{-1}

Table 2: Physical constants used in the surface energy balance model.

The fixed points for various values of Q can be viewed in Fig. 10, which also shows the trajectories in phase space to the steady state corresponding to $Q = 200 \text{ W m}^{-2}$. Also in this complicated situation it is possible to derive an analytical expression for the three timescales (see (61)). A plot of the time-scales is presented in Fig. 12.

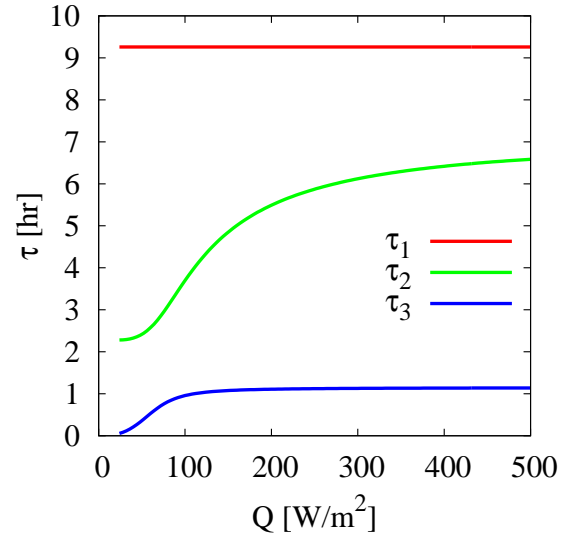


FIG. 12: The three timescales as a function of the net available energy Q .

6. CONCLUSIONS

- Mixed layers models capture the (slow) PBL dynamics quite well; the agreement with LES is very good.
- It is possible to derive analytical results for the steady state (fixed points) as a function of external conditions, as well as for the timescales of the dynamics.
- This in turn provides important information on the response of the PBL to changing conditions. Even in a

complicated situations where the surface fluxes follow from a surface energy balance can one determine the governing timescales.

- The internal timescales (e.g. of the PBL depth, mixed layer values of temperature and humidity) are generally much larger than the external timescales of the changing conditions and large scale forcings.

A. JACOBIAN OF A GENERIC SYSTEM

A generic system in terms of ζ , buoyancy θ_v

$$\frac{d\zeta}{dt} = w_e - w_s \quad (48)$$

$$\frac{d\theta_v}{dt} = \frac{\phi_v(1+c)}{\zeta} - w_s\Gamma_v \quad (49)$$

$$\frac{d\chi}{dt} = \frac{\phi_\chi + w_e\Delta_\chi}{\zeta} - w_s\Gamma_\chi \quad (50)$$

Here χ is extra scalar field which can influence the surface buoyancy flux, i.e. $\phi_v = \phi_v(\theta_v, \chi)$. The inversion jump of χ is given by

$$\Delta_\chi = \chi^{\text{FT}} + \Gamma_\chi\zeta - \chi$$

Fixed points relations are

$$\tilde{w}_e = w_s \quad (51)$$

$$\tilde{\zeta} = \frac{(1+c)\tilde{\phi}_v}{\Gamma_v w_s} \quad (52)$$

$$\tilde{\phi}_v = -w_s(\theta_v^{\text{FT}} - \tilde{\theta}_v) \quad (53)$$

$$\tilde{\phi}_\chi = -w_s(\chi^{\text{FT}} - \tilde{\chi}) \quad (54)$$

and depends clearly on the formulation of fluxes: prescribed values, coupled to the mixed layer values via a transfer rate, or fully coupled via a energy budget. It is useful to define

$$\begin{aligned} P_{vv} &= -\frac{1}{w_s} \frac{\partial \phi_v}{\partial \theta_v} & P_{v\chi} &= -\frac{1}{w_s} \frac{\partial \phi_v}{\partial \chi} \\ P_{\chi v} &= -\frac{1}{w_s} \frac{\partial \phi_\chi}{\partial \theta_v} & P_{\chi\chi} &= -\frac{1}{w_s} \frac{\partial \phi_\chi}{\partial \chi} \end{aligned}$$

After some algebra one finds that Jacobian in the fixed point to be given by:

$$\mathbf{J} = \begin{bmatrix} \frac{1+c}{c} & \Gamma_v & \frac{1+c}{c} \frac{\tilde{\Delta}_\chi}{\zeta} \\ \frac{1+c}{\Gamma_v} \left(P_{vv} - \frac{1}{c} \right) & (1+c)P_{v\chi} & \frac{1+c}{\Gamma_v} \left(P_{v\chi} - \frac{1}{c} \right) \frac{\tilde{\Delta}_\chi}{\zeta} \\ \frac{1+c}{\Gamma_v} \left(P_{\chi v} + \frac{1+c}{\Gamma_v} \left(P_{\chi v} - \frac{1}{c} \right) \right) & (1+c)P_{\chi\chi} & \frac{1+c}{\Gamma_v} \left(P_{\chi\chi} + 1 + \frac{1+c}{\zeta} \frac{P_{v\chi}}{\Gamma_v} \right) \frac{\tilde{\Delta}_\chi}{\zeta} \end{bmatrix} \quad (55)$$

For the case of a passive scalar buoyancy is not influenced by χ , hence $P_{v\chi} = 0$. By virtue of the two zeros in the right column of \mathbf{J} (55), the eigenvalue problem is decoupled ,

$$\lambda_{1,2} = -\frac{1+c}{2\tau_s} \left[\left(P_{vv} + \frac{1}{c} \right) \pm \sqrt{\left(P_{vv} - \frac{1}{c} \right) \left(P_{vv} - \frac{1-3c}{(1+c)c} \right)} \right] \quad (56)$$

$$\lambda_3 = -\frac{1}{\tau_s} [P_{\chi\chi} + 1] \quad (57)$$

When ϕ_χ is prescribed both $P_{\chi\chi}$ and $P_{\chi v} = 0$, so reducing the third eigenvalue to $\lambda_3 = -\tau_s^{-1}$, so the associated time scale is exactly τ_s . In the interactive case of $\phi_\chi = -w_t(\chi - \chi_s)$ it becomes $\lambda_3 = -(1 + w_t/w_s)/\tau_s$, hence $\tau_3 = \tau_s/(1 + w_t/w_s)$. In the former case the value of the flux ϕ_χ does not influence the time scale. In the latter case (interactive flux), an increased transfer rate does reduce the time scale.

The more complicated case of section 4.2, however, involves a coupling of the wind u to buoyancy via modu-

lation of the surface buoyancy flux $\phi_v = -c_d u(\theta_v - \theta_{vs})$. The system simplifies a little by choosing $\chi = c_d u$ (rather than $\chi = u$), which entails $\phi_\chi = -\chi^2$ and $\phi_v = -\chi(\theta_v - \theta_{vs})$. If we define $p = \tilde{\chi}/w_s = c_d \tilde{u}/w_s$, i.e. the ratio between the steady state transfer velocity and subsidence (see section 3), we get

$$\begin{aligned} P_{vv} &= p & P_{v\chi} &= -\frac{1}{w_s^2} \frac{\tilde{\phi}_v}{p} \\ P_{\chi v} &= 0 & P_{\chi\chi} &= 2p \end{aligned}$$

In steady state we furthermore have $\tilde{\Delta}_\chi = \tilde{\chi}^2/w_s = w_s p^2$. One ends up with

$$\tilde{\mathbf{J}} = -\frac{1}{\tau_s} \begin{bmatrix} \frac{1+c}{c} & \frac{1+c}{\Gamma_v} \left(p - \frac{1}{c}\right) & -\frac{\tau_s}{p} \\ \Gamma_v & (1+c)p & -\frac{\Gamma_v \tau_s}{p} \\ \frac{1+c}{c} \frac{p^2}{\tau_s} & \frac{1+c}{\Gamma_v} \left(p - \frac{1}{c}\right) \frac{p^2}{\tau_s} & p+1 \end{bmatrix} \quad (58)$$

The general expression for the corresponding eigenvalues can be computed easily by using symbolic programs like maple or Mathematica, but are too lengthy to be listed here. A special case, however, that can be done directly is when $p = 1/c$.

$$\lambda_\mu = -\frac{1}{\tau_s} \left[\frac{1+c}{c} + \eta_\mu \frac{\sqrt{1+c}}{c} \right] \quad \eta = \{0, i, -i\} \quad (59)$$

Finally we turn to the more complicated case where the sensible and latent heat surface fluxes follow from a surface energy balance. Here it is worthwhile to exploit the fact that χ can be chosen at will. One may choose χ such that $\tilde{\Delta}_\chi = 0$ which simplifies the Jacobian (55) considerably.

$$\tilde{\mathbf{J}} = -\frac{w_s}{\tilde{\chi}} \begin{bmatrix} \frac{1+c}{c} & \frac{1+c}{\Gamma_v} \left(P_{vv} - \frac{1}{c}\right) & \frac{1+c}{\Gamma_v} P_{v\chi} \\ \Gamma_v & (1+c)P_{vv} & (1+c)P_{v\chi} \\ 0 & P_{\chi v} & P_{\chi\chi} + 1 \end{bmatrix}$$

For the case where the subsidence profile is not constant but linearly increasing via $w_s = Dz$, one finds the Jacobian in the fixed point to be given by:

$$\tilde{\mathbf{J}} = -D \begin{bmatrix} \frac{2+3c}{c} & \frac{2(1+c)}{\Gamma_v} \left(P_{vv} - \frac{1}{c}\right) & \frac{2(1+c)}{\Gamma_v} P_{v\chi} \\ \Gamma_v & (1+c)P_{vv} & (1+c)P_{v\chi} \\ 0 & P_{\chi v} & P_{\chi\chi} + 1 \end{bmatrix} \quad (60)$$

where again we made the choice to set $\tilde{\Delta}_\chi = 0$. The

characteristic polynomial becomes

$$-c\lambda^2 + (c^2 P_{vv} + c(P_{vv} + P_{xx}) + 2 + 3c) \lambda \quad (61)$$

$$-2(1+c)(1 + P_{vv} + P_{xx}) - c(1+c)P_{vv} = 0 \quad (62)$$

$$\lambda = D \quad (63)$$

which shows that $\lambda = D$ can be factored out.

ACKNOWLEDGMENTS

This work was sponsored by the National Computing Facilities Foundation (NCF) for the use of supercomputer facilities, with financial support of NWO.

REFERENCES

- Ball, F. K., 1960: Control of the inversion height by surface heating. *Quarterly Journal of the Royal Meteorological Society*, **86** (370), 483–494.
- Heus, T., et al., 2010: Formulation of and numerical studies with the Dutch Atmospheric Large-Eddy Simulation (DALES). *Geoscientific Model Development*, **3** (1), 99–180.
- Lilly, D. K., 1968: Models of cloud-topped mixed layers under a strong inversion. *Quarterly Journal of the Royal Meteorological Society*, **94** (401), 292–309.
- Tennekes, H., 1973: A model for the dynamics of the inversion above a convective boundary layer. *Journal of the Atmospheric Sciences*, **30** (4), 558–566.
- van Driel, R. and H. J. J. Jonker, 2010: Convective boundary layers driven by nonstationary surface heat fluxes. *Journal of the Atmospheric Sciences*, **68**, 727–738.
- van Heerwaarden, C. C., J. V.-G. de Arellano, A. F. Moene, and A. A. M. Holtslag, 2009: Interactions between dry-air entrainment, surface evaporation and convective boundary-layer development. *Quart. J. Roy. Met. Soc.*, **135** (642, Part A), 1277–1291, doi: 10.1002/qj.431.
- Vilà-Guerau de Arellano, J., B. Gioli, F. Miglietta, H. J. J. Jonker, H. K. Baltink, R. W. A. Hutjes, and A. A. M. Holtslag, 2004: Entrainment process of carbon dioxide in the atmospheric boundary layer. *Journal of Geophysical Research*, **109**.